Structure and Computational Bases for Backbone Rearrangement in Marine Oxasqualenoids

Francisco Cen-Pacheco^{†,‡}, Adrián J. Santiago-Benítez[†], Ka Yi Tsui[§], Dean J. Tantillo^{§,*}, José J. Fernández^{†,*}, Antonio Hernández Daranas^{⊥,*}

- † Instituto Universitario de Bio-Organica Antonio González (IUBO-AG), Departmento de Química Orgánica, University of La Laguna, Av. Astrofísico Francisco Sánchez 2, 38206, Tenerife, Spain
- ‡ Facultad de Bioanálisis, Campus-Veracruz, Universidad Veracruzana, 91700, Veracruz, México
- § Department of Chemistry, University of California-Davis, Davis, CA 95616 USA
- ¹ Instituto de Productos Naturales y Agrobiología del CSIC (IPNA-CSIC), La Laguna, 38206, Tenerife, Spain

Supporting Information Placeholder

ABSTRACT: Six novel oxasqualenoids (polyether triterpenes) were isolated from the red alga *Laurencia viridis*. Laurokanols A-E (1-5), comprise an unreported tricyclic core with a [6,6]-spiroketal system. Yucatecone (6) shows a biogenetically intriguing epimerization at C14. Quantum mechanical calculations were used to corroborate their structures and to explain key steps involved in the biogenetic mechanisms proposed for the formation of oxasqualenoids.

INTRODUCTION

Red algae of the genus Laurencia are one of the most prolific sources of secondary metabolites known so far. Indeed, more than a thousand different compounds have been isolated from this genus. In addition, a vast array of notable bioactivities has been reported for these molecules.¹ Triterpene polyethers, also known as oxasqualenoids, represent one of the most interesting groups of metabolites isolated from Laurencia.² This group of molecules has shown interesting cytotoxic properties by targeting integrins and more recently antifouling, amoebicidal and antikinetoplastid activities.³⁻⁶ Their structural diversity and complexity derive from different cyclization reactions as a consequence of a chemical reaction cascade. Oxasqualenoids likely arise from a common precursor, (10R,11R) squalene epoxide, were isolated from L. okamurai. The later would be further oxidized into (6S,7S,10R,11R,14R,15R,18S,19S) squalene tetraepoxide as a common intermediate. Next, different squalene cyclizations have been proposed to proceed by a sophisticated multistep carbocation cascade, generating a large number of different compounds. However, it is difficult to explain the formation of certain intricate compounds by this classic sequential cascade, therefore establishing their biosynthetic pathway presents a great challenge.^{2,8,9}

As part of a project dedicated to the search of bioactive molecules from *Laurencia* that has been underway for long time,²⁻⁹ we have isolated and elucidated the structure of six unreported oxasqualenoids, named laurokanols A-E and yucatecone, from *L. viridis* (**Figure 1**). Their discovery is significative from a biosynthetic point of view. Thus, laurokanols comprise a novel tricyclic core that can be considered a key biogenetic intermediate to explain the intriguing configuration observed at C-14 in

yucatecone. Density-functional theory (DFT) calculations were performed to understand their biosynthetic pathway.

RESULTS AND DISCUSSION

Laurokanol A (1) showed a pseudomolecular ion at m/z609.2751/611.2755 [M+Na]⁺ (calcd 609.2731/611.2744) in its HRESIMS spectrum, which corresponds to a molecular formula of C₃₀H₅₁O₆Br. Analysis of COSY and TOCSY spectra, confirmed the existence of five ¹H—¹H spin systems: H3—H5, H7—H₂9, H11—H₂13, H₃28—H18 and H₂20—H-22. A comparison of its NMR data with those reported for the lead compound dehydrothyrsiferol (7) indicated that differences were located in two spin systems within the C11—C18.³ All fragments were linked making use of the HMBC correlations of the methyl groups C1, C24, C25, C26, C27, C28, C29 and C30. Thus, the presence of a 3-bromo-2,2,6-trimethyl-oxane ring, together with a dioxabicyclo [4,4,0] decane core and a 2-hydroxy-isopropyl-oxolane ring, was confirmed. All these structural motifs were previously found in other oxasqualenoids isolated from L. viridis.³ However, a distinctive spiroketal functionality in 1 was established on the basis of the correlations of the ketal quaternary carbon C-14 with H₂12, H₂13, H15, H₂16, H18 and H₃28. The dipolar correlations between H_3 -1/H-3, H-3/H-5 α , H_3 - $25/H_3-26$, H-7/H-11, H-8 β /H₃-27 and H-9 α /H-11 confirmed the relative configuration relationship within the A and B oxane rings as $3R^*,6S^*,7R^*,10S^*,11R^*$. In addition, correlations between H-12β/H₃-27, H-13β/H₃-27 and H-13β/H₃-28 indicated that the orientation of the [6,6]-spiroketal ring can only be explained by $14R^*$ and $15R^*$ (**Figure 1**). The relative configuration for the tetrahydropyran rings of the [6,6]-spiroketal system, was confirmed from the analysis of ${}^{3}J_{HH}$ values determined in TOCSY-1D experiment, that were measured in benzene-d6, due to signal overlapping in CDCl₃ (SI). To verify the previous conclusions about the relative configurations at C14 and C15, ¹H and ¹³C chemical shifts calculations using density functional theory (DFT) were performed. 10-12 Thus, computational models of the four possible candidate diasteroisomers (1a-1d in Figure 2) of the tricyclic core of 1 were optimized and conformational searches were performed for each one using a hybrid MCMM/low-mode sampling scheme and the MMFF94 force field. Afterward, conformers within a 20 kJ/mol threshold of the best minimum found were geometrically optimized and their Boltzmann weighted magnetic shielding constants were calculated at the B3LYP/6-31G(d,p) level. 13 Statistical analysis was done by linear regression of the calculated values ($\delta_{\text{scaled}} = (\sigma_{\text{calc}})$ - intercept)/slope) against experimental ones to correct possible bias introduced by systematic errors. The results were evaluated using three parameters, the correlation coefficient (R²), the corrected mean absolute error (CMAE), and the maximum absolute error (MaxErr).¹⁴ Conventionally, MaxErrs within ranges of 5-6 ppm and 0.3 ppm are considered acceptable for ¹³C and ¹H chemical shifts. According to our results, isomer **1a** gave the best outcomes for all parameters (Figure 2 and SI). In addition, the J-DP4 probability was calculated, 15 This method uses Bayes's theorem to estimate the probability that the chosen structure is correct by comparing calculated and experimental chemical shifts and ³J_{HH} values. J-DP4 gave a best match for isomer 1a with over 99.9% probability for the configuration. Finally, a comparison between the chemical shifts of the tetrahydrofuran rings of laurokanol A (1) and dehydrothyrsiferol (7)

resulted in almost identical values suggesting identical relative configurations ($19R^*$, $22R^*$).

(1a)
$$14R^*$$
, $15R^*$
(1b) $14R^*$, $15S^*$
(1c) $14S^*$, $15R^*$
(1d) $14S^*$, $15S^*$
HO $\overset{\circ}{H}$ OH

Isomer	MaxErr		CN	IAE	R^2		
	¹³ C	^{1}H	¹³ C	^{1}H	¹³ C	¹ H	
1a	2.92	0.17	0.90	0.07	0.998	0.977	
1b	5.55	0.54	1.52	0.17	0.994	0.924	
1c	4.46	0.57	1.62	0.24	0.994	0.864	
1d	5.60	0.64	1.91	0.32	0.992	0.815	

Figure 2. Model substructures (C6—C19) used to perform DFT calculations of the four C14—C15 possible diasteroisomers of laurokanol A (1). Statistical parameters obtained for the correlations of experimental *vs* calculated ¹H and ¹³C chemical shifts. MaxErr is the maximum absolute error. CMAE is the corrected mean absolute error and R² is the correlation coefficient.

Four closely related metabolites, laurakonols B-E (2-5), were also found in this study. Comparison of their NMR data indicated that all of them (1-5) share the same carbon backbone, but that 2-4 incorporated additional functional groups (-OH, -Br and -Cl) at C14 and C15. Assignment of the relative configuration at C-15 as S^* in 2 was based on the observation of a key correlation between H₃-27 and H₂-28, while in 3 and 4, C15 it was established as R^* by the dipolar correlation between H-17 and H₂-28. All other configurations remained identical to 1. (Figure 3). Stereochemical assignments were supported by QM-NMR calculations. Accordingly, calculated J-DP4 probabilities for the previously proposed configurations were over 95% in all cases (see SI). This approach was particularly useful to verify the configuration of 3 and 4, as proton overlapping in their mixture prevented clear ${}^{3}J_{\rm HH}$ measurements or may shed some doubt over the H17-H28 NOE correlation. It has to be noted that model compounds were similar to those used for compound 1 (figure 2) but introducing the corresponding modifications at C15 and C28 and excluding from the analysis all NMR data obtained for C28 and H28 due to the presence of halogens at that position.

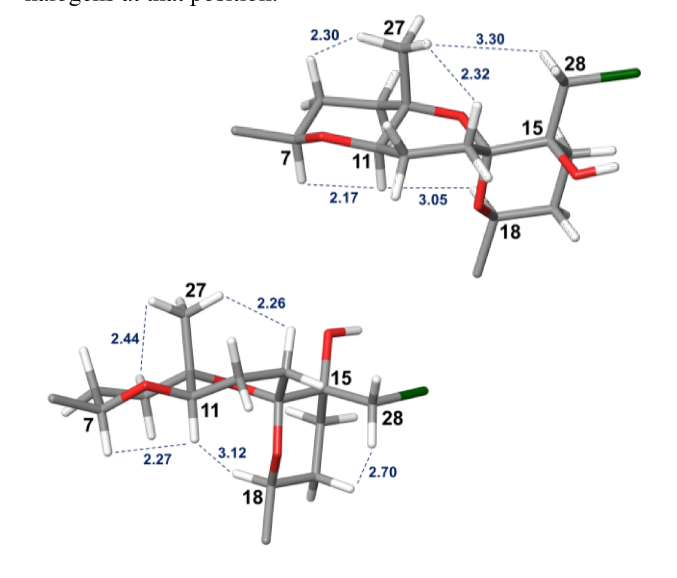


Figure 3. NOESY correlations for laurokanol B (2) - top - and C (3) - bottom -. Distances are shown in Å (blue dashes).

Table 1. ¹H NMR Data of Compounds 1–6

No	1ª	1 ^b	2ª	<i>3</i> °a	4ª	5ª	6 ^a
1	1.25, s	1.32, s	1.25, s	1.25, s	1.25, s	1.12, s	1.27, s
2	-	-	-	-	-	-	-
				3.85, dd	3.85, dd		
3	3.85, dd	3.81, dd	3.83, dd	(4.1,	(4.1,	3.71, t	3.90, dd
	(4.1, 12.3)	(4.0, 12.5)	(4.1, 12.5)	12.4)	12.4)	(7.6)	(4.0, 12.3)
							2.09, dddd
	2.07, dddd	1.91, dddd	2.08, dddd	2.08, m	2.08, m		(3.5, 4.0, 4.3,
	(3.6,4.1,4.3,13.2)	(4.0, 4.0, 4.0, 13.4)	(3.7, 4.1, 4.0,				13.3)
4	2.21, dddd	2.09, dddd	13.3)	2.22, m	2.22, m	1.78, m	2.25, dddd
	(3.9, 12.3, 13.2,	(2.0, 12.5, 13.4,	2.23, dddd	2.22, 111	,		(3.9, 12.0, 13.3,
	13.8)	13.4)	(3.7, 13.1, 13.2, 13.3)				13.5)
	1.48, ddd	1.52, ddd	1.46, ddd	1.44, m	1.44, m	1.67, m	1.55, ddd
	(4.3, 13.8, 13.8)	(4.0, 13.4, 13.4)	(4.0, 13.1, 13.9)	1.11, 111	1.11, 111	1.07, 111	(4.3, 13.5, 13.6)
5	1.77, ddd	1.73, ddd	1.76, dt	1.76, m	1.76, m	2.01, ddd	1.80, dd
	(3.6, 3.9, 13.8)	(2.0, 4.0, 13.4)	(3.7, 3.7, 13.9)	1.70, 111	,	(8.4, 11.5, 12.1)	(3.5, 3.9, 13.6)
6		_	_	_	_	-	-
Ū				2.05.44	3.05, dd		
7	3.06, dd	3.28, dd	3.05, dd	3.05, dd (2.5,	(2.5,	3.30, dd	3.09, d
•	(2.4, 11.4)	(2.6, 11.8)	(2.5, 11.6)	11.6)	11.6)	(2.6, 11.8)	(2.4, 11.2)
	1.43, dddd	1.48, dddd	1.45, dddd		,	1.51, dddd	
	(2.6,11.4, 13.5,	(2.9, 11.8, 13.5,	(4.5, 11.6, 12.3,	1.46, m	1.46, m	(2.9, 11.8, 13.5,	1.53, m
8	13.5)	13.5)	13)			13.5)	
	1.73, dddd	1.82, dddd	1.74, dddd	1.78, m	1.78, m	1.69, dddd	1.76, m
	(2.4, 3.0, 4.3, 13.5)	(2.6, 2.9, 4.5, 13.5)	(2.5, 2.7, 4.3, 13)			(2.6, 2.9, 4.5, 13.5)	
	1.59, ddd	1.80, ddd	1.61, ddd	1.65, m	1.65, m	1.65, ddd	1.50, m
	(4.3, 12.2, 13.5)	(4.5, 12.7, 13.5)	(4.3, 12.3, 12.3)	,	,	(4.5, 12.7, 13.5)	ŕ
9	1.78, ddd	1.90, ddd	1.78, ddd	1.84, m	1.84, m	1.83, ddd	1.70, m
	(2.6, 3.0, 12.2)	(2.9, 2.9, 12.7)	(4.5, 2.7, 12.3)	110 1, 111		(2.9, 2.9, 12.7)	,
10	-	-	-	-	-	-	-
	3.96, dd	4.22, dd	3.91, dd	3.87, dd	3.87, dd	4.03, dd	3.00, dd
11	(8.1, 9.8)	(8.0, 10.0)	(8.1, 9.8)	(7.8,10.4)	(7.8,10.4)	(8.1, 10.0)	(3.8, 11.8)
	(***,****)	· · · · · · · · · · · · · · · · · · ·		(7.0,10.7)	(,)	1.42, dddd	1.51, dddd
	1.35, dddd	1.50, dddd	1.40, dddd	1.43, m	1.43, m	· ·	(3.2, 3.8, 4.0, 12.2)
12	(1.0, 9.8, 11.2, 13.5)	(1.3, 10.0, 11.1, 13.0)	(1.3, 9.8, 11.1, 13.0)			(1.3, 10.0, 11.1, 13.0)	1.64, dddd
-	1.87, dddd	2.07, dddd	1.88, dddd	1.83, m	1.83, m	1.93, dddd	(2.9, 11.8, 12.0,
	(8.0, 8.1, 10.5, 13.5)	(7.7, 8.0, 10.5, 13.0)	(7.7, 8.1, 10.5, 13.0)			(7.5, 8.1, 10.4, 13.0)	12.2)
			, , , , ,			(, , , , , , , , , , , , , , , , , , ,	1.37, dddd
	1.55, ddd	1.48, ddd	1.95, ddd	1.62, m	1.68, m	1.58, ddd	(4.0, 11.7, 12.0,
	(1.0, 10.5, 14.2)	(1.3, 10.5, 14.1)	(1.3, 10.5, 14.1)	1.02, 111	1.00, 111	(1.3, 10.4, 14.1)	12.0)
13	2.17, ddd	2.03, ddd	2.04, ddd	2.19, m	2.19, m	2.19, ddd	1.65, dddd
	(8.0, 11.2, 14.2)	(7.7,11.1, 14.1)	(7.7,11.1, 14.1)	2.19, 111	2.17, 111	(7.5,11.1, 14.1)	(2.1, 2.9, 3.2,
	(***, ****, * ****)	(,,,,,,,,,,,,,,,,,,,,,,,,,,,,,,,,,,,,,,	(,,,,,,,,,,,,,,,,,,,,,,,,,,,,,,,,,,,,,,			(7.3,11.1, 14.1)	12.0)
							3.47, dd
14	-	-	-	-	-	-	(2.1; 4.6; 11.7)
		1.25, ddt				1.38, ddt	(2.1, 4.0, 11.7)
15	1.35, m	(3.8, 6.7, 6.7, 6.7,	_	_	_	(3.8, 6.7, 6.7, 6.7,	1.44, m
13	1.55, III	12.5)				(3.8, 6.7, 6.7, 6.7, 12.5)	1.77, 111
						1.42, dddd	
					1.04	1.12, uuuu	
	1.38, m	1.33, dddd	1.85 ddd	1.80, m	1.84, m		1.34, m
	1.56, dddd	1.33, dddd (2.9, 3.8, 4.4, 13.0)	(4.3, 13.1, 13.4)	1.80, m		(2.9, 3.8, 4.4, 13.0)	
	1.56, dddd (4.1, 13.0, 13.0,	1.33, dddd (2.9, 3.8, 4.4, 13.0) 1.70, dddd	(4.3, 13.1, 13.4) 1.91 ddd	1.80, m 2.17, m	2.17, m	(2.9, 3.8, 4.4, 13.0) 1.57, dddd	1.34, m 1.73, m
	1.56, dddd	1.33, dddd (2.9, 3.8, 4.4, 13.0)	(4.3, 13.1, 13.4)			(2.9, 3.8, 4.4, 13.0)	
	1.56, dddd (4.1, 13.0, 13.0, 13.0)	1.33, dddd (2.9, 3.8, 4.4, 13.0) 1.70, dddd (4.2, 12.5, 13.0, 13.0)	(4.3, 13.1, 13.4) 1.91 ddd (5.5, 5.5, 13.4)	2.17, m	2.17, m	(2.9, 3.8, 4.4, 13.0) 1.57, dddd (4.2, 12.5, 13.0, 13.0)	1.73, m
	1.56, dddd (4.1, 13.0, 13.0, 13.0) 1.18, dddd	1.33, dddd (2.9, 3.8, 4.4, 13.0) 1.70, dddd (4.2, 12.5, 13.0, 13.0) 1.12, dddd	(4.3, 13.1, 13.4) 1.91 ddd (5.5, 5.5, 13.4) 1.47, dddd			(2.9, 3.8, 4.4, 13.0) 1.57, dddd (4.2, 12.5, 13.0, 13.0) 1.20, dddd	1.73, m 2.56, ddd
16	1.56, dddd (4.1, 13.0, 13.0, 13.0)	1.33, dddd (2.9, 3.8, 4.4, 13.0) 1.70, dddd (4.2, 12.5, 13.0, 13.0)	(4.3, 13.1, 13.4) 1.91 ddd (5.5, 5.5, 13.4)	2.17, m 1.24, m	2.17, m 1.24, m	(2.9, 3.8, 4.4, 13.0) 1.57, dddd (4.2, 12.5, 13.0, 13.0)	1.73, m 2.56, ddd (5.8, 9.7, 17.7)
16	1.56, dddd (4.1, 13.0, 13.0, 13.0) 1.18, dddd (4.1, 12.5, 12.5,	1.33, dddd (2.9, 3.8, 4.4, 13.0) 1.70, dddd (4.2, 12.5, 13.0, 13.0) 1.12, dddd (4.4, 12.5, 12.5,	(4.3, 13.1, 13.4) 1.91 ddd (5.5, 5.5, 13.4) 1.47, dddd (3.7, 5.5, 13.1,	2.17, m	2.17, m	(2.9, 3.8, 4.4, 13.0) 1.57, dddd (4.2, 12.5, 13.0, 13.0) 1.20, dddd (4.4, 12.5, 12.5,	1.73, m 2.56, ddd (5.8, 9.7, 17.7) 2.71, ddd
16	1.56, dddd (4.1, 13.0, 13.0, 13.0) 1.18, dddd (4.1, 12.5, 12.5, 13.0)	1.33, dddd (2.9, 3.8, 4.4, 13.0) 1.70, dddd (4.2, 12.5, 13.0, 13.0) 1.12, dddd (4.4, 12.5, 12.5, 13.0)	(4.3, 13.1, 13.4) 1.91 ddd (5.5, 5.5, 13.4) 1.47, dddd (3.7, 5.5, 13.1, 13.4)	2.17, m 1.24, m	2.17, m 1.24, m	(2.9, 3.8, 4.4, 13.0) 1.57, dddd (4.2, 12.5, 13.0, 13.0) 1.20, dddd (4.4, 12.5, 12.5, 13.0)	1.73, m 2.56, ddd (5.8, 9.7, 17.7)
16	1.56, dddd (4.1, 13.0, 13.0, 13.0) 1.18, dddd (4.1, 12.5, 12.5, 13.0) 1.53, m	1.33, dddd (2.9, 3.8, 4.4, 13.0) 1.70, dddd (4.2, 12.5, 13.0, 13.0) 1.12, dddd (4.4, 12.5, 12.5, 13.0) 1.44, dddd (2.4, 2.9, 4.2, 12.5)	(4.3, 13.1, 13.4) 1.91 ddd (5.5, 5.5, 13.4) 1.47, dddd (3.7, 5.5, 13.1, 13.4) 1.50, dddd (5.5, 4.3, 11.1, 13.4)	2.17, m 1.24, m 1.56, m	2.17, m 1.24, m 1.56, m	(2.9, 3.8, 4.4, 13.0) 1.57, dddd (4.2, 12.5, 13.0, 13.0) 1.20, dddd (4.4, 12.5, 12.5, 13.0) 1.55, dddd (2.3, 2.9, 4.2, 12.5)	1.73, m 2.56, ddd (5.8, 9.7, 17.7) 2.71, ddd
16 17	1.56, dddd (4.1, 13.0, 13.0, 13.0) 1.18, dddd (4.1, 12.5, 12.5, 13.0)	1.33, dddd (2.9, 3.8, 4.4, 13.0) 1.70, dddd (4.2, 12.5, 13.0, 13.0) 1.12, dddd (4.4, 12.5, 12.5, 13.0) 1.44, dddd	(4.3, 13.1, 13.4) 1.91 ddd (5.5, 5.5, 13.4) 1.47, dddd (3.7, 5.5, 13.1, 13.4) 1.50, dddd	2.17, m 1.24, m	2.17, m 1.24, m	(2.9, 3.8, 4.4, 13.0) 1.57, dddd (4.2, 12.5, 13.0, 13.0) 1.20, dddd (4.4, 12.5, 12.5, 13.0) 1.55, dddd	1.73, m 2.56, ddd (5.8, 9.7, 17.7) 2.71, ddd

19	-	-	-	-	-	-	-
20	1.52, ddd (2.8, 7.8, 11.8)	1.39, ddd (2.5, 7.6, 11.9)	1.59, ddd (2.5, 8.2, 11.8)	1.59, m	1.59, m	1.55, ddd (2.5, 7.6, 11.9)	1.77, m
	2.13, ddd (8.7, 11.7, 11.8)	2.12, ddd (8.5, 11.5, 11.9)	2.14, ddd (8.2, 8.3, 11.8)	2.03, m	2.03, m	2.16, ddd (8.5, 11.5, 11.9)	2.16, m
21		1.60, dddd	1.80, m	1.79, m	1.79, m		
	1.79, m	(2.5, 5.9, 8.5, 12.5) 1.78, dddd (7.6, 9.7, 11.5, 12.5)	1.84, m	1.84, m	1.84, m	1.80, m	1.83, m
22	3.74, dd (6.1, 9.3)	3.78, dd (5.9, 9.7)	3.74, dd (5.2, 9.8)	3.71, dd (5.3, 10.3)	3.71, dd (5.3, 10.3)	3.78, dd (5.7, 9.9)	3.77, dd (6.2, 8.7)
23	-	-	-	-	-	-	-
24	1.12, s	1.12, s	1.12, s	1.12, s	1.12, s	1.13, s	1.15, s
25	1.39, s	1.38, s	1.38, s	1.39, s	1.39, s	1.20, s	1.40, s
26	1.19, s	1.17, s	1.18, s	1.18, s	1.18, s	1.14, s	1.21, s
27	1.12, s	1.20, s	1.14, s	1.20, s	1.20, s	1.17, s	1.14, s
28	0.84, d	*	3.64, d (11.4)	3.78, d (11.7)	3.66, d (10.9)	0.87, d	0.88, d
	(6.5)	(6.7)	3.75 d (11.4)	3.65, d (11.7)	3.57, d (10.9)	(6.6)	(6.8)
29	1.12, s	1.04, s	1.16, s	1.14, s	1.14, s	1.15, s	1.33, s
30	1.26, s	1.32, s	1.26, s	1.26, s	1.26, s	1.28, s	1.26, s

Chemical shifts are in ppm and J values in Hz are in parentheses. ^a Measured in CDCl3. ^b Measured in benzene-d6.

Differently, laurokanol E (5) does not incorporate any halogen atom in its structure and ring A was contracted to an oxolane ring with an isopropanol append, instead of the bromine-containing pyran observed for 1-4. The relative configurations within the oxolane ring were determined on the basis of the observation of 1-3 NOE correlations between H-3 and H-5 $_{\alpha}$ as well as between H-5 $_{\beta}$ and H₃-26. In addition, the great correspondences between the ¹H and ¹³C chemical shifts of the C1—C6 portion of 5 and those reported for an identical moiety found in pseudodehydrothyrsiferol set the relative configurations as 3*S** and 6*S**. In All other stereocentres within 5 were established as identical to those of 1 based on dipolar correlations, coupling constant values and QM-NMR calculations (Figure 3 and SI).

Yucatecone (6) turned out to be an isomer of the lead compound dehydrothyrsiferol (7), according to its molecular formula $C_{30}H_{51}O_6Br$ (ESI-HRMS m/z ion peak [M+Na]⁺ at 609.2772 and 611.2760) and NMR data. The combined study of COSY, HSQC and HMBC spectra confirmed the presence of all the characteristic cyclic system observed in dehydrothyrsiferol (7). However, NMR data of 6 revealed differences in the C11-C19 moiety, such as the substitution of the typical olefinic protons H_228 ($\delta_H 4.88/5.05$) by a methyl group ($\delta_H 0.88$), the absence of the proton H18 by oxidation of hydroxyl group on C18 ($\delta_{\rm C}$ 215.7 ppm) and a change in the chemical shifts of H11 and H14. The dipolar correlations observed in the NOESY experiment of yucatecone (6), in particular those observed between H₃1/H₃. H3/H5, H₃25/H₃26, H7/H11, H7/H8α and H₃27/H8β, supports that 6 possesses the same relative configuration within the A and B rings as in 7. However, the relative configuration of C14 was initially established as R^* from the observed correlations between H14 and H₃27. The epimerization of C14 represents the first example of this situation in all known thysiferol derivatives so far. This intriguing change led us to further structural studies to confirm the relative configurations at C14 and C15.

Thus, we used a *J*-based NMR configurational analysis (JBCA). ¹⁸ The measured values for $^3J_{\rm H14,H15} = 4.6$ Hz, $^3J_{\rm C28,H14} = 3.8$ Hz, $^3J_{\rm C13,H15} = 3.3$ Hz, $^3J_{\rm C16,H14} = 2.2$ Hz and $^2J_{\rm C14,H15} = -4.8$ Hz, obtained from homodecoupling experiments, HSQC-HECADE, and *J*-HMBC spectra indicated unequivocally the presence of a conformational equilibrium anti—gauche—with configuration *erythro* (**Figure 4** and **SI**). **Ref** Finally, the oxidation of 7 with pyridinium chlorochromate in anhydrous CH_2Cl_2 yielded the oxidate compound, 18-ketodehydrothyrsiferol, that shows almost identical 1H and ^{13}C chemical shift values from C18-C24 as **6**, supporting that the new compound shares the same configuration in that moiety (**SI**).

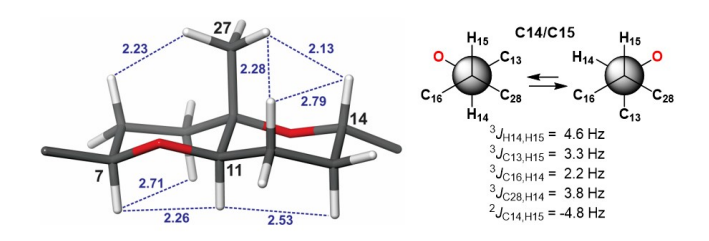


Figure 4. Key dipolar correlations observed within the bicyclic core of yucatecone (6) and a summary of the *J*-based NMR configurational analysis around the C14-C15 bond.

The complex structures of these novel oxaesqualenoids are difficult to explain by the classic sequential cascade cyclizations of squalene-10-11 oxide.⁵⁻⁷ Laurokanols **1-5** are the first examples of polyether triterpenes possessing a tricyclic core including a [6,6]-spiroketal system and **6** shows an intriguing epimerization in the asymmetric position C14. Therefore, we propose

a biosynthetic pathway starting from dehydrothirsiferol (7), the most abundant secondary metabolite found in $L.\ viridis$.

Scheme 1. General biosynthetic pathway proposed for compounds 1-6.

Allylic oxidation of the dehydrothyrsiferol (7) would be the key step on the construction of other oxasqualenoids, such as 16-hydroxidehydrothyrsiferol and its C16 epimer as well as the intermediate 14-hydroxy derivative of 14-ketodehydrothyrsiferol.^{5,7}The keto form of the last metabolite, would evolve by dehydration to yield the thyrsenol series of compounds and the oxidative cleavage between C14 and C15 in the thyrsenols would yield the adejene series of compounds comprising a C17 backbone.^{7,19} Alternatively, ketalization of the carbonyl C14 of 14-ketodehydrothyrsiferol, would lead to the formation of the laurokanol series of compounds in a similar way to that observed in avermectin and corozalic acid.^{20,21} Yucatecone (6) would be synthetized from protonation of the oxygen atom at C18 that results in the fragmentation of the spiroketals system in laurokanols with the concomitant formation of the oxonium intermediate, followed by hydride migration form C18 to C14. This would result in the formation of a ketone at C18 and inversion of the C14 configuration due to a hydride migration (Scheme 1).

To test these hypotheses, we investigated the mechanisms using DFT calculations (carried out using Gaussian09).²² Structural optimizations and frequency calculations were performed at two levels for comparison purposes: PCM(water)-B3LYP(D3)//6-31+G(d,p)^{13,23,24} and PCM(water)-M06-2X//6-31+G(d,p).²⁵ All computed transition state structures (TSS) were confirmed to have a single imaginary frequency and IRC calculations were used to confirm which minima were connected to each TSS.²⁶ Conformational searches were performed on each flexible structure using Spartan10 (the Merck Molecular Force Field, MMFF, was used in a systematic search).²⁷ The resulting conformers were first subjected to single-point energy calculations at the PCM(water)-B3LYP(D3)//6-31+G(d,p) level and then conformers within 4 kcal/mol of the lowest energy conformer were fully optimized. To reduce computational cost, we truncated the system as shown in Scheme 2, assuming the truncated parts do not interfere with the reactions of interest.

We began by modeling the cyclization of protonated 14-ketodehydrotyrsiferol. The carbonyl carbon at position C14 is susceptible to attack by either the hydroxyl group at C10 or the hydroxyl group C18, leading to pathway A (**Figure 5**, top) or pathway B (**Figure 5**, bottom), respectively. Each attack can, in principle, also occur from the *si* or *re* face of the C14 carbonyl.

Scheme 2. Truncation of 14-Ketodehydrothyrsiferol. To reduce computational cost, parts of the structure that are likely irrelevant to the mechanisms of interest were replaced by methyl groups.

We discuss first pathway A. Formation of INTA(R) is predicted to be ~11 kcal/mol uphill and is accompanied by a barrier of ~14 kcal/mol (**Figure 5**, top) at the PCM(water)-M06-2X//6-31+G(d,p) level of theory (green). The formation of INTA(S) is predicted to be much less endergonic (only ~3 kcal/mol) and to be associated with a lower barrier of ~12 kcal/mol (**Figure 5**, top). Thus, although both reactions are kinetically feasible at biological temperatures, attacking on the si face of C-14 is favored. This conclusion persists when using PCM(water)-B3LYP(D3)//6-31+G(d,p) calculations instead, although specific energies differ (**Figure 5**, black). Solvent-assisted dehydration (not modeled) then occurs to form INT2A, an overall exergonic process from protonated 14-ketodehydrotyrsiferol. Deprotonation of INT2A affords thyrsenol.

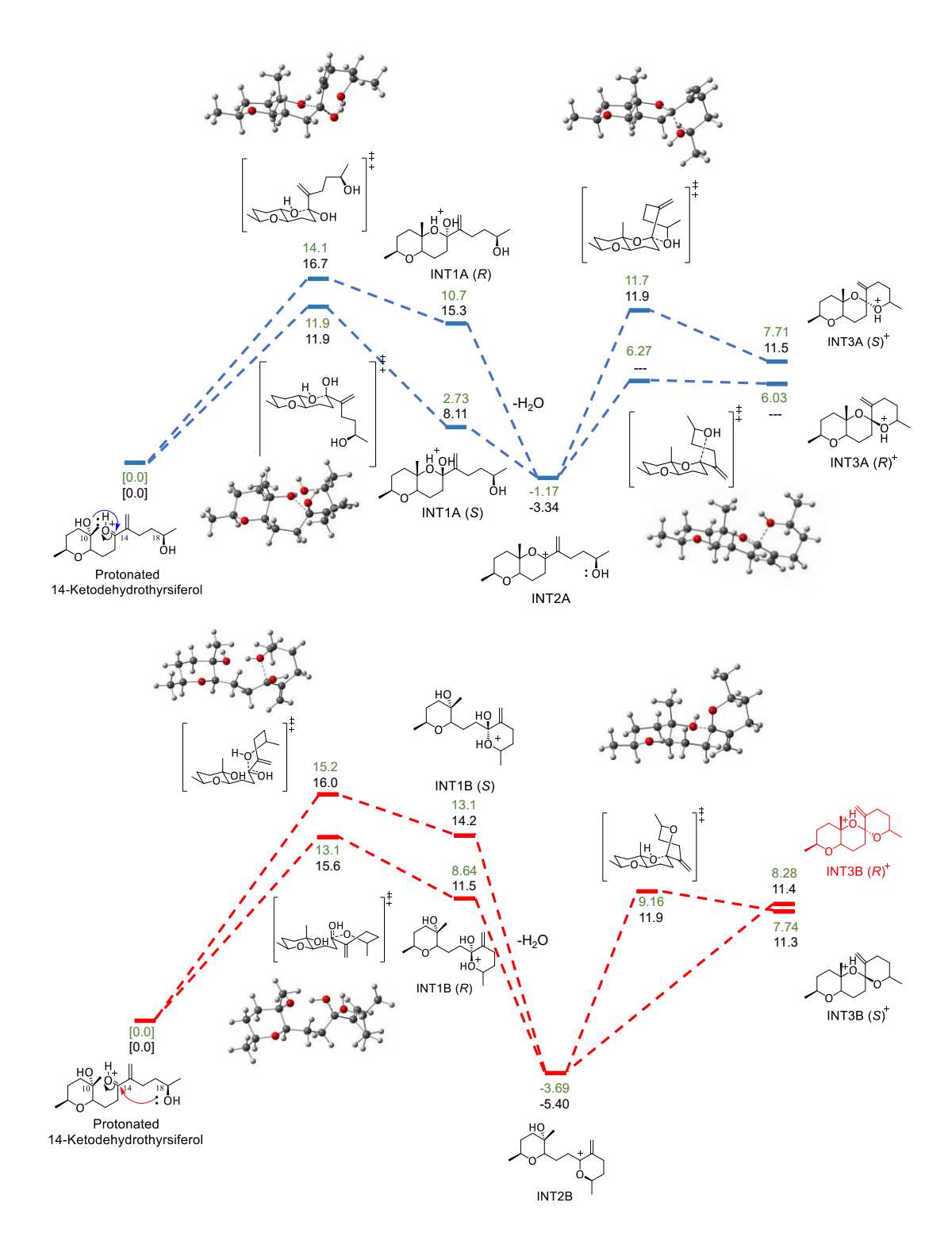


Figure 5. Free energy diagrams for pathways A (top) and B (bottom). Energies are calculated using PCM(water)-M06-2X//6-31+G(d,p) (green) and PCM(water)-B3LYP(D3)//6-31+G(d,p) (black). Diagram is scaled to the green energies. The starting material, protonated 14-ketodehydrothyrsiferol, is set as the relative zero. Units are in kcal/mol. For pathway A, INT3A(R)⁺ failed to optimize as a minimum at PCM(water)-B3LYP(D3)//6-31+G(d,p). And for pathway B, INT3B(S)⁺ failed to optimize as a minimum using both methods, hence its free energies are resulted from constrained optimization with C14 – O18 restricted to 1.58 Å.

Table 2. ¹³C NMR Data of Compounds 1–6

No	1 ^a	1 ^b	2 a	3ª	4 a	5 ^a	6 ^a
					•		
1	31.2	31.3	31.1	31.2	31.2	24.0	31.6
2	75.0	75.2	75.0	75.1	75.1	70.5	75.1
3	59.4	59.3	59.0	59.1	59.1	86.4	59.3
4	28.4	28.6	28.2	28.4	28.4	26.3	28.3
5	37.2	37.5	37.0	37.2	37.2	35.5	37.7
6	74.9	74.8	74.4	74.5	74.5	83.9	74.5
7	86.0	86.4	85.8	86.1	86.1	83.2	87.0
8	23.3	23.7	23.1	23.4	23.4	24.5	23.5
9	38.7	39.2	38.2	38.5	38.5	38.7	38.1
10	72.0	72.3	73.5	74.0	74.0	71.8	72.4
11	75.6	75.9	75.0	75.0	75.0	75.5	81.3
12	20.3	20.7	19.7	19.4	19.4	20.2	24.9
13	27.9	28.2	23.6	23.2	23.2	27.8	28.5
14	99.1	99.4	100. 0	99.9	99.9	99.0	72.8
15	38.8	39.1	71.5	72.3	71.6	38.6	37.5
16	27.4	27.7	28.0	28.4	29.9	27.2	26.4
17	27.1	27.4	21.8	24.8	24.8	27.0	35.1
18	74.6	75.0	74.2	74.9	74.9	74.5	215. 7
19	84.8	84.7	84.3	84.1	84.1	84.7	88.8
20	32.9	33.2	32.3	32.7	32.7	32.6	35.3
21	26.3	26.9	26.5	26.7	26.7	26.6	26.2
22	87.1	87.6	87.3	87.4	87.4	87.0	87.6
23	70.2	70.2	69.9	70.1	70.1	70.0	70.7
24	24.6	24.9	24.5	24.7	24.7	24.4	24.7
25	23.7	23.9	23.6	23.7	23.7	27.5	24.3
26	20.1	20.1	19.9	20.1	20.1	22.5	20.7
27	19.7	19.9	19.7	19.7	19.7	19.5	14.9
28	17.1	17.3	51.7	47.4	37.4	16.9	15.6
29	24.5	24.3	24.6	24.7	24.7	24.4	24.7
30	28.7	28.5	28.6	28.6	28.6	28.4	27.6
^a Measured in CDCl3. ^b Mesured in benzene- <i>d</i> 6.							

INT2A can also cyclize to form INT3A(R) and INT3A(S). Again, selectivity is predicted with PCM(water)-M06-2X//6-31+G(d,p) (barriers of ~7 vs. ~13 kcal/mol; **Figure 5**, top, green). While the kinetic preference predicted here favors the relative configuration of the epimer of laurokanol, cyclizations to form both epimers are predicted to be endergonic and reversible (note that ring opening of INT3A(R)⁺ is predicted have a miniscule barrier, for example, consistent with the fact that we were unable to locate a minimum corresponding to INT3A(R)⁺ with PCM(water)-B3LYP(D3)//6-31+G(d,p)), indicating that product selectivity would be controlled by deprotonation (which was not modeled due to problems in appropriately treating the explicit solvent that would be involved).

We also considered the possibility that laurokanol was formed via initial attack of the hydroxyl group at C18 onto the C14 carbonyl (pathway B; **Figure 5**, bottom). This pathway is similar in its energetics to pathway A, indicating that either pathway is energetically viable. For pathway B, however, we were unable to locate a minimum corresponding to $INT3B(R)^+$ with either theoretical method used, i.e., ring-opening is predicted

to be barrierless (the ultimate in reversibility!; the relative energy of $INT3B(R)^+$ is estimated from a calculation with the C14 - O18 constrained to 1.58 Å). In addition, while such preferences can be overcome once enzymes are involved, we predict that laurokanol is ~5 kcal/mol lower in energy than its epimer, which is consistent with the relative configuration found in the backbones of all experimentally isolated laurokanols. We also examined the proposal that yucatacone can arise from laurokanol (Scheme 1). We predict that laurokanol is susceptible to rapid ring-opening in acidic environments. The ring-opening energy surface is predicted to be very flat at the PCM(water)-M06-2X//6-31+G(d,p) level (**Figure 6**, green) and we were not able to optimize laurokanol with O18 protonated as a minimum with PCM(Water)-B3LYP(D3)//6-31+G(d,p) (the starred energy in Figure 6 reflects a constrained optimization with the bond between C14 and O18 forced to remain closed). Intramolecular hydride transfer is predicted to be possible, although our predicted barriers with PCM(Water)-B3LYP(D3)//6-31+G(d,p) are clearly high for non-enzymatic biologically-relevant processes. Barriers from PCM(water)-M06-2X//6-31+G(d,p) calculations are lower. If the actual barriers are somewhere between the estimates from these two levels of theory, then they would be at the high end of the range of barriers generally associated with biological relevance.²⁸. Given the error bars expected for such methods and the small difference in predicted barriers for forming protonated yucatecone versus its epimer, it is likely than an enzyme is necessary for producing the observed product with high selectivity.

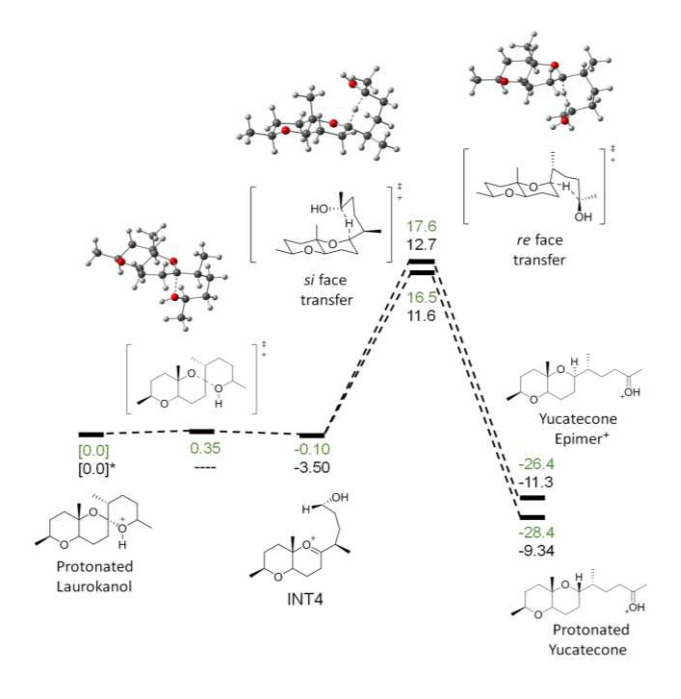


Figure 6. Free energy diagram for yucatecone formation. Energies are calculated using PCM(water)-M06-2X//6-31+G(d,p) (green) and PCM(water)-B3LYP(D3)//6-31+G(d,p) (black). Protonated laurokanol is set as the relative zero and units are in kcal/mol. Protonated laurokanol is not a minimum with PCM(water)-B3LYP(D3)//6-31+G(d,p), therefore its free energy was estimated by constrained optimization.

CONCLUSIONS

Six new marine oxasqualenoids (1-6) were isolated from the red algae Laurencia viridis collected in the Canary Islands. Laurokanols A-E (1-5), comprise a novel tricyclic core with a [6,6]-spiroketal system not previously described to our best knowledge. From a biogenetic point of view, yucatecone (6) shows an intriguing epimerization at C14. Yucatecone is the first compound of these series with an R^* configuration at the mentioned position. Therefore, the discovery of these compounds is relevant from a biosynthetically perspective. Computational methods were used to set the bases to explain the backbone rearrangements observed in these oxasqualenoids. Although our results indicate that the proposed mechanisms are kinetically feasible, an enzyme is likely involved for controlling stereselectivity, especially in the formation of yucatecone. Thus, we have demonstrated that the proposed connection between dehydrothirsiferol, laurokanol and yucatecone series are energetically viable.

EXPERIMENTAL SECTION

General Experimental Procedures. All solvents used were HPLC-grade. HPLC chromatography was monitored by TLC, performed on silica gel Merck 60 F254. TLC plates were visualized by UV light (365 nm) and phosphomolybdic acid solution 10 wt % in methanol. Optical rotation was determined on a Perkin-Elmer 241 polarimeter using a sodium lamp operating at 589 nm. The IR spectrum was measured on a Bruker IFS55 spectrometer, using a chloroform solution to place a film of the compounds on the NaCl disk. NMR spectra were performed on Bruker AVANCE 500 or 600 MHz instruments at 300 K, and coupling constants are given in Hz. Structural assignments were made with additional information from gCOSY, 1D/2D gTOCSY, gHSQC, gNOESY and gHMBC experiments using standard pulse sequences. Phase-sensitive NOESY spectra were measured using a mixing time of 500 ms and TOCSY experiments using mixing times ranging from 10 to 100 ms. ³J_{H,H} values were measured from 1D ¹H NMR or 1D TOCSY when signal overlapping not permitted it. NMR data were processed using Topspin or MestReNova software. Mass spectra were recorded on a Waters Micromass LCT Premier XE mass spectrometer.

Extraction and Isolation. Specimens of L. viridis were collected in the intertidal zone at Paraiso Floral, Tenerife, Canary Islands (28°07'12"'N, 16°46'45"'W) and frozen at -80 °C until their extraction. 20.75 Kg of fresh algae was extracted using CHCl₃:MeOH (1:1) at room temperature followed by solvent evaporation under reduced pressure a dark-green viscous oil was obtained (83.0 g). The chromatographic separation started using Sephadex LH-20 (7 × 50 cm) and CH₂Cl₂/MeOH (1:1) as mobile phase. The fraction collected between 225-360 mL (53.5 g) was subsequently processed using silica gel column (7 × 50 cm) using a linear gradient of n-hexane/EtOAc (4:1—1:4), and the fraction collected between 350-500 mL was dried (10.71 g). Next, Lobar LiChroprep RP-18 chromatography using MeOH/H2O (9:1) afforded a fraction of 4.43 g by collecting the volume eluted between 105-160 mL. Next, this fraction was chromatographed by a medium pressure silica gel chromatography Lobar LiChroprep-Si60 with CH₂Cl₂:acetone (8:2) as eluent; the fractions collected between 80 and 105 mL were combined to give a 770 mg fraction. Final purification was carried out by HPLC employing a μ -Porasil column using n-hexane/AcOEt/CH₂Cl₂/MeOH (65:18:15:2), to afford laurokanol A (1) (8.4 mg) and two fractions that were further purified using n-hexane/acetone 19:1 and 9:1, respectively, to afford laurokanol B (2) (0.84 mg), the mixture of laurokanol C (3) and laurokanol D (4) (0.49 mg) as well as laurokanol E (5) (0.37 mg) and yucatecone (6) (4.4 mg).

Laurokanol A (1): Amorphous, white solid; $[α]^{25}_D + 24$ (c 0.33, CHCl₃); IR V_{max} (film): 2973, 2873, 1462, 1378, 1122 and 1093 cm⁻¹; ¹H NMR (600 MHz, CDCl₃) and ¹³C NMR (125 MHz, CDCl₃), Tables 1 and 2; HRESIMS m/z 609.2751/611.2755 [M+Na]⁺ (calcd for $C_{30}H_{51}O_6^{81}$ BrNa, 611.2746).

Laurokanol B (2): Amorphous, white solid; $[α]^{25}_D$ -35 (*c* 0.084, CHCl₃); IR V_{max} (film): 3297, 2919, 2357, 1640, 1264, 1041 and 731 cm⁻¹; ¹H NMR (600 MHz, CDCl₃) and ¹³C NMR (125 MHz, CDCl₃), Tables 1 and 2; HRESIMS m/z 659.2344/661.2305/663.2283 [M+Na]⁺, (calcd for $C_{30}H_{50}O_7^{79}Br^{35}CINa$, 659.2326).

Laurokanol C and D (3/4): Amorphous, white solid; IR $V_{\rm max}$ (film): 3356, 2930, 2364, 1640, 1262, 1053 and 795 cm⁻¹; ¹H NMR (600 MHz, CDCl₃) and ¹³C NMR (125 MHz, CDCl₃), Tables 1 and 2; HRESIMS m/z 659.2308 /661.2276/663.2224 [M+Na]⁺ (calcd for $C_{30}H_{50}O_7^{79}Br^{35}ClNa$, 659.2326) and 703.1803/705.1827/ 707.1818 [M+Na]⁺ (calcd for $C_{30}H_{50}O_7^{79}Br_2Na$, 707.1821).

Laurokanol E (**5**): Amorphous, white solid; $[α]^{25}_D$ -47 (*c* 0.037, CHCl₃); IR V_{max} (film): 3300, 2970, 1458, 1234, 1051 and 800 cm⁻¹; ¹H NMR (600 MHz, CDCl₃) and ¹³C NMR (125 MHz, CDCl₃), Tables 1 and 2; HRESIMS m/z 547.3605 [M+Na]⁺ (calcd for C₃₀H₅₂O₇Na, 547.3605).

Yucatecone (6): Amorphous, white solid; $[α]^{25}_D + 32$ (c 0.44, CHCl₃); IR $V_{\rm max}$ (film): 2977, 2874, 1714, 1590, 1381, 1129 and 1101 cm⁻¹; NMR data ¹H (600 MHz, CDCl₃) and ¹³C NMR (125 MHz, CDCl₃), Tables 1 and 2. HRESIMS $[M+Na]^+$ m/z 609.2772, 611.2760 (Calcd 611.2746 for $C_{30}H_{51}O_6^{81}BrNa$).

QM-NMR calculations. All calculations were done following the general protocols previously described for J-DP4 methods. Molecular mechanics conformational searches were undertaken using the Macromodel software (Schrödinger Inc.) and the MMFF94 force field.²⁹ Solvation effects of CHCl₃ were simulated using the generalized Born/surface area (GBSA) solvation model. Extended nonbonded cutoff distances (Van der Waals cutoff of 8.0 Å and an electrostatic cutoff of 20.0 Å) were used. All local minima within 20 kJ of the global minimum were saved, and the analysis of the results was undertaken using Maestro software. Quantum mechanical calculations were carried out using the Gaussian 09 package.²² Structure optimizations were done at the B3LYP/6-31G (d) level of theory. Magnetic shielding constants (σ) were calculated by means of the gauge including atomic orbitals (GIAO) method, 30 at the B3LYP/6-31G(d,p) level of theory as recommended for J-DP4. Unscaled chemical shifts (δ_u) were calculated using TMS as reference standard according to the following expression $\delta_u = \sigma_0 - \sigma_x$, where σ_x is the Boltzmann averaged shielding tensor (over all significantly populated conformations) and σ_0 is the shielding tensor of TMS computed at the same level of theory used to calculate σ_x . Boltzmann averaging was done according to eq1:

$$\sigma^{x} = \frac{\sum_{i} \sigma_{i}^{x} e^{(-E_{i}/RT)}}{\sum_{e} e^{(-E_{i}/RT)}}$$
 (equation 1)

where σ^x is the shielding constant for nucleus x in conformer i, R is the molar gas constant (8.3145 J K $^{-1}$ mol $^{-1}$), T is the temperature used for the calculation (298 K), and E_i is the relative energy of conformer i (to the lowest energy conformer) obtained from a single-point NMR calculation at the corresponding level of theory. The scaled chemical shifts (δ_s) were computed as $\delta_s = (\delta_u - b)/m$, where m and b are the slope and intercept, respectively, resulting from a linear regression calculation on a plot of δ_u against δ_{exp} . The corrected mean absolute error (CMAE) and the maximum absolute error (MaxErr) were calculated as follows, CMAE = $(\Sigma_i | \delta_{exp} - \delta_{scaled} | /n)/b$, where δ_{exp} are the experimental chemical shifts and MaxErr = $\max(|\delta_{exp} - \delta_{scaled}|)$. Proton chemical shifts for each methyl group were averaged due to their conformational freedom.

Computational Stationary Point Analysis.

All computations were carried out at the B3LYP-D3/6-31+G(d,p)^{13,23,24} and M06-2X/6-31+G(d,p)²⁵ level of theories, including an implicit solvent environment (PCM-water). Structures are confirmed to be minima by frequency analysis. Transition state structures were also confirmed to have relevant imaginary vibrational modes. IRC calculations were used to confirm the minima connected to each TSS.²⁶ Conformational searches were performed on each flexible structure using Spartan10 (the Merck Molecular Force Field, MMFF, was used in a systematic search).²⁷ The resulting conformers were first subjected to single-point energy calculations at the PCM(water)-B3LYP(D3)//6-31+G(d,p) level and then conformers within 4 kcal/mol of the lowest energy conformer were fully optimized using both methods.

ASSOCIATED CONTENT

Supporting Information

The Supporting Information is available free of charge on the ACS Publications website.

HR-ESI-MS, ¹H, ¹³C, selective 1D TOCSY and 2D NMR spectra of compounds **1-6**. Cartesian coordinates, energies, NMR calculated data and J-DP4 analysis results for model compounds and transition states used in structural elucidation and biosynthetic analyses of compounds **1-6**.

AUTHOR INFORMATION

Corresponding Author

Notes

The authors declare no competing financial interest.

ACKNOWLEDGMENT

This research was funded by the Spanish Ministry of Science and Innovation (PID2019-109476RB-C21), Cooperation Programme INTERREG-MAC 2014-2020 (MAC2/1.1b/279, AHIDAGRO), FEDERCB-220206 (Consejo Nacional de Ciencia y Tecnología,

CONACyT) and the National Science Foundation (CHE-1856416 and supercomputing resources from the XSEDE program via CHE-030089). This study made use of the SGAI-CSIC supercomputing facilities. A.J.S.B thanks the CajaCanarias foundation for a grant.

REFERENCES

- (1) (a) Harizani, M.; Ioannou, E.; Roussis, V. The Laurencia Paradox: An Endless Source of Chemodiversity. In *Progress in the chemistry of organic natural products*; 2016; Vol. 102, pp 91–252. (b) Carroll, A. R.; Copp, B. R.; Davis, R. A.; Keyzers, R. A.; Prinsep, M. R. Marine Natural Products. *Nat. Prod. Rep.* 2020, 37 (2), 175–223 and previous articles in the same series.
- (2) (a) Fernández, J. J.; Souto, M. L.; Norte, M. Marine polyether triterpenes. *Nat. Prod. Rep.* 2000, 17, 235-246. (b) Morimoto, Y. The Role of Chemical Synthesis in Structure Elucidation of Oxasqualenoids. *Org. Biomol. Chem.* 2008, 6, 1709-1719.
- (3) Cen-Pacheco, F.; Santiago-Benítez, A. J.; García, C.; Álvarez-Méndez, S. J.; Martín-Rodríguez, A. J.; Norte, M.; Martín, V. S.; Gavín, J. A.; Fernández, J. J.; Daranas, A. H. Oxasqualenoids from Laurencia Viridis: Combined Spectroscopic-Computational Analysis and Antifouling Potential. J. Nat. Prod. 2015, 78 (4), 712–721.
- (4) Lorenzo-Morales, J.; Díaz-Marrero, A. R.; Cen-Pacheco, F.; Sifaoui, I.; Reyes-Batlle, M.; Souto, M. L.; Daranas, A. H.; Piñero, J. E.; Fernández, J. J. Evaluation of Oxasqualenoids from the Red Alga Laurencia Viridis against Acanthamoeba. *Mar. Drugs* 2019, 17 (7).
- (5) Díaz-Marrero, A. R.; López-Arencibia, A.; Bethencout-Estrella, C. J.; Cen-Pacheco, F.; Sifaoui, I.; Hernández Creus, A.; Duque-Ramírez, M. C.; Souto, M. L.; Hernández Daranas, A.; Lorenzo-Morales, J.; et al. Antiprotozoal Activities of Marine Polyether Triterpenoids. *Bioorg. Chem.* 2019, 92, 103276.
- (6) Cen-Pacheco, F.; Villa-Pulgarin, J. A.; Mollinedo, F.; Norte, M.; Daranas, A. H.; Fernández, J. J. Cytotoxic Oxasqualenoids from the Red Alga *Laurencia viridis*. Eur. J. Med. Chem. 2011, 46, 3302-3308.
- (7) (a) Kigoshi, H.; Ojika, M.; Shizuri, Y.; Niwa H.; Yamada, K. (10R, 11R)-(+)-squalene-10, 11-epoxide: Isolation from Laurencia okamurai and the Asymmetric Synthesis. Tetrahedron Lett., 1982, 5413-5414. (b) Cen-Pacheco, F.; Pérez Manríquez, C.; Luisa Souto, M.; Norte, M.; Fernández, J.; Hernández Daranas, A. Marine Longilenes, Oxasqualenoids with Ser-Thr Protein Phosphatase 2A Inhibition Activity. Mar. Drugs 2018, 16 (4), 131.
- (8) Cen-Pacheco, F.; Nordstrom, L.; Souto, M. L.; Norte, M.; Fernandez, J. J.; Daranas, A. H. Studies on Polyethers Produced by Red Algae. *Mar. Drugs* 2010, 8, 1178-1188.
- (9) Cen-Pacheco, F.; Mollinedo, F.; Villa-Pulgarín, J. A.; Norte, M.; Fernández, J. J.; Hernández Daranas, A. Saiyacenols A and B: The Key to Solve the Controversy about the Configuration of Aplysiols. *Tetrahedron* 2012, 68 (36), 7275–7279.
- (10) Cen-Pacheco, F.; Rodríguez, J.; Norte, M.; Fernández, J. J.; Daranas, A. H. Connecting Discrete Stereoclusters by Using DFT and NMR Spectroscopy: The Case of Nivariol. *Chem. Eur. J.* 2013, 19, 8525-8532.
- (11) Domínguez, H. J.; Crespín, G. D.; Santiago-Benítez, A. J.; Gavín, J. A.; Norte, M.; Fernández, J. J.; Daranas, A. H. Stereochemistry of Complex Marine Natural Products by Quantum Mechanical Calculations of NMR Chemical Shifts: Solvent and Conformational Effects on Okadaic acid. *Mar. Drugs* 2014, 12, 176-192.
- (12) Lodewyk, M. W.; Siebert, M. R.; Tantillo, D. J. J., Computational Prediction of ¹H and ¹³C Chemical Shifts: A Useful Tool for Natural Product, Mechanistic, and Synthetic Organic Chemistry. *Chem. Rev.* 2012, 112, 1839-1862.
- (13) (a) Becke, A. D. Density-functional thermochemistry. III. The role of exact exchange. *J. Chem. Phys.* 1993, 98, 5648–5652.
 (b) Lee, C.; Yang, W.; Parr, R. G. Development of the Colle-

- Salvetti correlation-energy formula into a functional of the electron density. *Phys. Rev. B: Condens. Matter Mater. Phys.* **1988**, *37*, *785*–789. (c) Miehlich, B.; Savin, A.; Stoll, H.; Preuss, H. Results obtained with the correlation energy density functionals of becke and Lee, Yang and Parr. *Chem. Phys. Lett.* **1989**, *157*, *200*–206.
- (14) Saielli, G.; Nicolaou, K. C.; Ortiz, A.; Zhang, H.; Bagno, A. Addressing the Stereochemistry of Complex Organic Molecules by Density Functional Theory-NMR: Vannusal B in retrospective. J. Am. Chem. Soc. 2011, 133, 6072-6077.
- (15) Grimblat, N.; Gavín, J. A.; Hernández Daranas, A.; Sarotti, A. M. Combining the Power of J Coupling and DP4 Analysis on Stereochemical Assignments: The J-DP4 Methods. *Org. Lett.* 2019, 21 (11), 4003–4007.
- (16) Napolitano, J. G.; Gavín, J. A.; García, C.; Norte, M.; Fernández, J. J.; Daranas, A. H. On the Configuration of Five-Membered Rings: A Spin-Spin Coupling Constant Approach. Chem. - A Eur. J. 2011, 17 (23), 6338–6347.
- (17) Cen-Pacheco, F., Villa-Pulgarin, J. A., Mollinedo, F., Norte Martín, M., Fernández, J. J., Hernández Daranas, A. New Polyether Triterpenoids from *Laurencia viridis* and Their Biological Evaluation. *Mar. Drugs* 2011, 9, 2220-2235.
- (18) Matsumori, N.; Kaneno, D.; Murata, M.; Nakamura, H.; Tachibana, K. Stereochemical Determination of Acyclic Structures Based on Carbon- Proton Spin-Coupling Constants. A Method of Configuration Analysis for Natural Products. J. Org. Chem. 1999, 64 (3), 866–876.
- (19) Norte, M.; Fernandez, J. J., Souto, M. L.; Gavin, J. A.; Garcia-Gravalos, M. D. Thyrsenols A and B, Two Unusual Polyether Squalene Derivatives. *Tetrahedron*, **1997**, 53, 3173-3178.
- (20) Ikeda, H.; Omura, S. Avermectin Biosynthesis. Chem. Rev. 1997, 97, 2591-2609.
- (21) Napolitano, J. G.; Norte, M.; Fernandez, J. J.; Hernandez Daranas, A. Corozalic Acid: A Key Okadaic Acid Biosynthetic Precursor with Phosphatase Inhibition Activity. *Chem. Eur. J.* 2010, 16, 11576-11579.
- (22) Frisch, M. J.; Trucks, G. W.; Schlegel, H. B.; Scuseria, G. E.; Robb, M. A.; Cheeseman, J. R.; Scalmani, G.; Barone, V.; Mennucci, B.; Petersson, G. A.; et al. *Gaussian 09, Revision D.*

- 01; Gaussian, Inc.: Wallingford, CT, USA, 2010.
- (23) (a) Grimme, S.; Antony, J.; Ehrlich, S.; Krieg, H. A consistent and accurate ab initio parametrization of density functional dispersion correction (DFT-D) for the 94 elements H-Pu. J. Chem. Phys. 2010, 132, 154104. (b) Grimme, S.; Ehrlich, S.; Goerigk, L. Effect of the damping function in dispersion corrected density functional theory, J. Comp. Chem. 2011, 32, 1456.
- (24) Cammi, R.; Mennucci, B.; Tomasi, J. In Computational Chemistry: Reviews of Current Trends; Leszczynski, J., Ed.; World Scientific Publishing Co. Pte. Ltd.: Singapore, 2003; Vol. 8.
- (25) (a) Zhao, Y.; Truhlar, D. G. The M06 suite of density functionals for main group thermochemistry, thermochemical kinetics, noncovalent interactions, excited states, and transition elements: two new functionals and systematic testing of four M06-class functionals and 12 other functionals. Theor. Chem. Acc. 2008, 120, 215-241. (b) Walker, M.; Harvey, J. A.; Sen, A.; Dessent, C. E. H. Performance of M06, M06-2X, and M06-HF Density Functionals for Conformationally Flexible Anionic Clusters: M06 Functionals Perform Better than B3LYP for a Model System with Dispersion and Ionic Hydrogen-Bonding Interactions, J. Phys. Chem. A. 2013, 117, 47, 12590-12600
- (26) (a) Fukui, K. The Path of Chemical Reactions The IRC Approach, Acc. Chem. Res. 1981, 14, 363-368. (b) Gonzalez, C.; Schlegel, H. B. Reaction Path Following in Mass-Weighted Internal Coordinates. J. Phys. Chem. 1990, 94, 5523-5527.
- (27) Spartan, Version10 (Wavefunction, Ind.: Irvine, CA, USA2010).
- (28) Wang, S. C.; Tantillo, D. J. J. Theoretical Studies on Synthetic and Biosynthetic Oxidopyrylium—Alkene Cycloadditions. Pericyclic Pathways to Intricarene, Org. Chem. 2008, 73, 1516-1523.
- (29) MacroModel Schrodinger release 2018-3; Schrodinger LLC: New York (2018).
- (30) (a) Ditchfield, R. J. Chem. Phys. 1972, 56, 5688-5691. b)
 Ditchfield, R. Mol. Phys.1974, 27, 789-807. c) Rohlfing, C. M.;
 Allen, L. C.; Ditchfield, R. Chem. Phys. 1984, 87, 9-15. d)
 Wolinski, K.; Hinton, J. F.; Pulay, P. J. Am. Chem. Soc. 1990, 112, 8251-8260.